crystals

MDPI

Article

Computer Simulation of the Incorporation of V^{2+}, V^{3+}, V^{4+}, V^{5+} and Mo^{3+}, Mo^{4+}, Mo^{5+}, Mo^{6+} Dopants in $LiNbO_3$

Romel Menezes Araujo [1,2], Emanuel Felipe dos Santos Mattos [1], Mário Ernesto Giroldo Valerio [3] and Robert A. Jackson [4,*]

1 Chemistry Coordination/IPISE/PIC, Pio Decimo College, Campus Jabotiana, Aracaju-SE 49027-210, Brazil; raraujoster@gmail.com (R.M.A.); manel12309@gmail.com (E.F.d.S.M.)
2 Research Institute—Instituto de Pesquisa, Tecnologia e Negócios-IPTN, Aracaju-SE 49095000, Brazil
3 Physics Department, Federal University of Sergipe, Campus Universitário, São Cristovão-SE 491000-000, Brazil; megvalerio@gmail.com
4 Lennard-Jones Laboratories, School of Chemical and Physical Sciences, Keele University, Keele, Staffordshire ST5 5BG, UK
* Correspondence: r.a.jackson@keele.ac.uk

Received: 10 March 2020; Accepted: 6 May 2020; Published: 1 June 2020

Abstract: The doping of $LiNbO_3$ with V^{2+}, V^{3+}, V^{4+} and V^{5+} as well as Mo^{3+}, Mo^{4+}, Mo^{5+} and Mo^{6+} ions is of interest in enhancing its photorefractive properties. In this paper, possible incorporation mechanisms for these ions in $LiNbO_3$ are modelled, using a new set of interaction potentials fitted to the oxides VO, V_2O_3, VO_2, V_2O_5 and to $LiMoO_2$, Li_2MoO_3, $LiMoO_3$, Li_2MoO_4.

Keywords: lithium niobate; divalent; trivalent; tetravalent; pentavalent and hexavalent doping; computer modelling

1. Introduction

Ferroelectric lithium niobate is a material that has been extensively studied because of its many technological applications, including optical integrated circuits, electro-optical modulators, optical memories, acoustic filters, high-frequency beam deflectors, frequency converters and holographic volume storage [1–9], for which holographic volume storage performance is very important [10–15]. This paper looks at the doping of $LiNbO_3$ with vanadium and molybdenum ions in different charge states, with the aim of predicting the optimum location of dopants, and charge compensation mechanisms where needed.

Previous work on vanadium and molybdenum doped lithium niobate has included experimental studies of how its photorefractive properties are enhanced by doping with molybdenum ions [16,17] where it is suggested that the Mo^{6+} ion dopes at the Nb^{5+} site. Another study looks at $LiNbO_3$ co-doped with Mg and V, concluding that some of the vanadium dopes at the Nb site in the 5+ charge state, but that $V^{4+}{}_{Li}$, $V^{3+}{}_{Li}$ and $V^{2+}{}_{Li}$ defects are also observed [18]. Finally, another recent publication [19] has looked at the photorefractive response of Zn and Mo co-doped $LiNbO_3$ in the visible region, and concluded that the presence of Mo^{6+} ions helps promote fast response and multi-wavelength holographic storage, which is attributed to their occupation of regular niobium sites in the lattice.

In a Density Functional Theory (DFT) study [20], vanadium doping was modelled, and it was concluded that vanadium substitutes at the Li^+ site as V^{4+}, but that it dopes at the Nb site as a neutral defect as the Fermi level is increased. In another DFT study [21], molybdenum doping was modelled and it was concluded that the most stable configuration involves doping at the Nb^{5+} site, in agreement with the previously mentioned experimental studies [16,17]. It is noted that in the DFT

studies, predictions were made on the basis of defect formation energies, as opposed to the solution energy approach adopted in this paper.

This paper presents a computer modelling study of V^{2+}, V^{3+}, V^{4+} and V^{5+} as well as Mo^{3+}, Mo^{4+}, Mo^{5+} and Mo^{6+} doping in $LiNbO_3$ using interatomic potentials. Such calculations enable predictions to be made of the sites occupied by dopant ions, and the form of charge compensation adopted, if needed. These calculations provide information about how the defects behave in the material, and how they influence its properties in the applications mentioned previously. It follows a series of papers by the authors on $LiNbO_3$ doped with a range of ions [22–27].

2. Materials and Methods

2.1. Interatomic Potentials

The interatomic potentials used in this work consist of Buckingham potentials, supplemented by an electrostatic term, as given below:

$$V(r_{ij}) = \frac{q_i q_j}{r_{ij}} + A_{ij} \exp\left(\frac{-r_{ij}}{\rho_{ij}}\right) - C_{ij} r_{ij}^{-6} \quad (1)$$

This expression shows that for each pair of ions it is necessary to determine three parameters: A_{ij}, ρ_{ij} and C_{ij}, which are constants for each interaction, q_i, q_j represent the charges of the ions i and j, and r_{ij} is the interatomic distance. The parameters are determined by empirical fitting, and formal charges are used for q_i and q_j. The procedure by which potentials were obtained for $LiNbO_3$ is explained in the work of Jackson and Valério [22], and the derivation of the potentials for the vanadium and molybdenum dopants is described in Section 3.1 below. The potentials for $LiNbO_3$ have been the subject of recent studies on the doping of the structure with rare earth ions [23,24], doping with Sc, Cr, Fe and In [25], metal co-doping [26] and doping with Hf [27]. These papers show that modelling can predict the energetically optimal locations of the dopant ions and calculate the energy involved in the doping process. This paper extends this procedure to the study of V^{2+}, V^{3+}, V^{4+} and V^{5+} as well as Mo^{3+}, Mo^{4+}, Mo^{5+} and Mo^{6+} doped lithium niobate, with the aim of establishing the optimal doping site and charge compensation scheme for both sets of ions.

2.2. Defect Formation Energies

The calculation of defect formation energies is carried out using the Mott–Littleton approximation [28], in which the crystal is divided into two regions: region I, which contains the defect, and region II, which extends from the edge of region I to infinity. In region I, the positions of the ions are adjusted until the resulting force is zero. The radius of region I is selected such that the forces in region II are relatively weak and the relaxation can be treated according to the harmonic response to the defect (a dielectric continuum). An interfacial region IIa is introduced to treat interactions between region I and region II.

3. Results and Discussion

3.1. Derivation of Interatomic Potential Parameters

It was necessary to derive potential parameters for the dopant oxide structures: VO, V_2O_3, VO_2 and V_2O_5 as well as $LiMoO_2$, Li_2MoO_3, Li_3MoO_4 and Li_2MoO_4. For V^{2+}-O^{2-}, V^{3+}-O^{2-}, V^{4+}-O^{2-} and V^{5+}-O^{2-} as well as Mo^{3+}-Li^+, Mo^{4+}-Li^+, Mo^{5+}-Li^+, Mo^{6+}-Li^+, Mo^{3+}-O^{2-}, Mo^{4+}-O^{2-}, Mo^{5+}-O^{2-} and Mo^{6+}-O^{2-} interactions, a new set of potentials was derived empirically by fitting to the observed structures as shown in Table 1. The O^{2-}-O^{2-} potential was obtained by Sanders et al. [29] and uses the shell model for O [30], which is a representation of ionic polarisability, in which each ion is represented by a core and a shell, coupled by a harmonic spring, and the Li-O potential was taken from [22]. In all cases, the dopant-oxide potentials were obtained by fitting to parent oxide structures.

Table 1. Interionic potentials obtained from a fit to the VO, V_2O_3, VO_2, V_2O_5, $LiMoO_2$, Li_2MoO_3, Li_3MoO_4 and Li_2MoO_4 structures.

Interaction	A_{ij}(eV)	ρ_{ij}(Å)	C_{ij}(Å^6 eV)
Li_{core}-O_{shell}	950.0	0.2610	0.0
V_{core}-O_{shell}	293.240087	0.475181	0.0
Mo_{core}-Li_{core}	573.532325	0.369602	0.0
Mo_{core}-$O^{2-}{}_{shell}$	3003.79	0.3474	0.0
Mo_{core}-O_{core}	600.263736	0.328558	0.0
$O^{2-}{}_{shell}$-$O^{2-}{}_{shell}$	22764.0	0.1490	27.88
Harmonic	**k(eV Å^2)**	**r_o(Å)**	
V_{core}-O_{core}	46.997833	1.942956	
Mo_{core}-O_{core}	385.638986	2.073074	
Species			Y(e)
Mo_{core}			3.0 4.0 5.0 6.0
V_{core}			2.0 3.0 4.0 5.0
O_{core}			0.9
O_{shell}			−2.9
Spring			k(Å^{-2} eV)
O_{core}-O_{oore}			70.0

Table 2 compares experimental and calculated structures of VO [31], V_2O_3 [32], VO_2 [33] and V_2O_5 [34] oxides as well as $LiMoO_2$ [35], Li_2MoO_3 [36], Li_3MoO_4 [37] and Li_2MoO_4 [38] lithium molybdate structures, using the potentials in Table 1. It is seen that the experimental and calculated lattice parameters differ by less than 1%, confirming that the potentials can be used in further simulations of defect properties. The calculations were carried at 0 K (the default for the modelling code and used in most other theoretical studies) and at 293 K for comparison with room temperature results. In this way, we can see how the structure and energies vary with temperature.

Table 2. Comparison of calculated (calc.) and experimental (expt.) lattice parameters.

Oxide	Lattice Parameter	Exp.	Calc. (0 K)	Δ%	Calc. (293 K)	Δ%
VO	a(Å) = b(Å) = c(Å)	4.067800	4.108237	0.99	4.10683	0.98
V_2O_3	a(Å) = b(Å) = c(Å)	9.393000	9.304757	0.90	9.346331	0.94
VO_2	a (Å) = b(Å)	4.556100	4.569483	0.20	4.566212	0.22
	c(Å)	2.859800	2.866421	0.23	2.857861	0.07
V_2O_5	a(Å)	11.971900	11.99652	0.20	12.01247	0.33
	b(Å)	4.701700	4.722561	0.44	4.660343	0.88
	c(Å)	5.325300	5.355671	0.57	5.371149	0.86
Lithium Molybdates	**Lattice Parameter**	**Exp.**	**Calc. (0 K)**	**Δ%**	**Calc. (293 K)**	**Δ%**
$LiMoO_2$	a(Å) = b(Å)	2.866300	2.880528	0.50	2.887246	0.73
	c(Å)	15.474300	15.409390	0.42	15.595024	0.78
Li_2MoO_3	a(Å) = b(Å)	2.878000	2.854443	0.82	2.859809	0.63
	c(Å)	14.91190	15.002886	0.61	15.04632	0.90
Li_3MoO_4	a(Å) = b(Å) = c(Å)	4.1389	4.107762	0.75	4.106941	0.77
Li_2MoO_4	a(Å) = b(Å)	14.330000	14.301305	0.20	14.384501	0.38
	c(Å)	9.584	9.492067	0.96	9.632413	0.96

3.2. Defect Calculations

In this section, calculated energies for dopant ions in $LiNbO_3$ are reported. The divalent, trivalent, tetravalent, pentavalent and hexavalent dopants can substitute at Li and Nb sites in the $LiNbO_3$ matrix with charge compensation taking place in a number of ways. The proposed schemes described in

the following subsections are written as solid state reactions using the Kroger–Vink notation [39]. This notation appears in the tables in Sections 3.2.1–3.2.5 where the dot/bullet (·) means a net positive charge and the dash/prime (′) means a net negative charge.

3.2.1. Divalent Dopants

The substitution of the divalent dopant V^{2+} in the Li^{+} and Nb^{5+} host sites requires a charge-compensating defect, which can involve Li and Nb vacancies, Nb_{Li} anti-sites, interstitial oxygen, self-compensation and oxygen vacancies. The modes of substitution considered for divalent cations are shown in Table 3.

Table 3. Types of defects considered due to M = V^{2+} incorporation in $LiNbO_3$.

Site	Charge Compensation	Reaction
Li^{+}	**Lithium Vacancies**	(i) $MO + 2\,Li_{Li} \rightarrow M_{Li} + V'_{Li} + Li_2O$
	Niobium Vacancies	(ii) $5MO + 5Li_{Li} + Nb_{Nb} \rightarrow 5M_{Li} + V''''''_{Nb} + 2.5Li_2O + 0.5Nb_2O_5$
	Oxygen Interstitial	(iii) $2MO + 2Li_{Li} \rightarrow 2M_{Li} + O''_i + Li_2O$
Li^{+} and Nb^{5+}	**Self-Compensation**	(iv) $4MO + 3\,Li_{Li} + Nb_{Nb} \rightarrow 3M_{Li} + M'''_{Nb} + 1.5Li_2O + 0.5\,Nb_2O_5$
Nb^{5+}	**Lithium Vacancies and Anti-site (Nb_{Li})**	(v) $MO + 2Li_{Li} + Nb_{Nb} \rightarrow M'''_{Nb} + V'_{Li} + Nb_{Li} + Li_2O$
	Anti-site (Nb_{Li})	(vi) $4MO + 3Li_{Li} + 4Nb_{Nb} \rightarrow 4M'''_{Nb} + 3Nb_{Li} + Li_2O + LiNbO_3$
		(vii) $4MO + 3Li_{Li} + 4Nb_{Nb} \rightarrow 4M'''_{Nb} + 3Nb_{Li} + 1.5Li_2O + 0.5Nb_2O_5$
	Oxygen Vacancies	(viii) $2MO + 2Nb_{Nb} + 3O_O \rightarrow 2M'''_{Nb} + 3V_O + Nb_2O_5$

The solution energies for the divalent (V^{2+}) dopant with different charge-compensating mechanisms were evaluated and plotted as a function of the reaction schemes. Based on the lowest energy value, it seems that the incorporation of a divalent (V^{2+}) ion is energetically favourable at the lithium and niobium sites, taking into account the first in relation to the c axis. In schemes (i) and (iv), the energy difference in eV is small at both temperatures in the first neighbours, indicating that it can be incorporated at the lithium site compensated by a lithium vacancy as well as by self-compensation as shown in Figure 1. This can be attributed to the similarity between the ionic radius of V^{2+}, which is 0.79 Å, and those of the Li^{+} site, which varies between 0.59 and 0.74 Å, and the Nb^{5+} site, which varies between 0.32 and 0.71 Å [40].

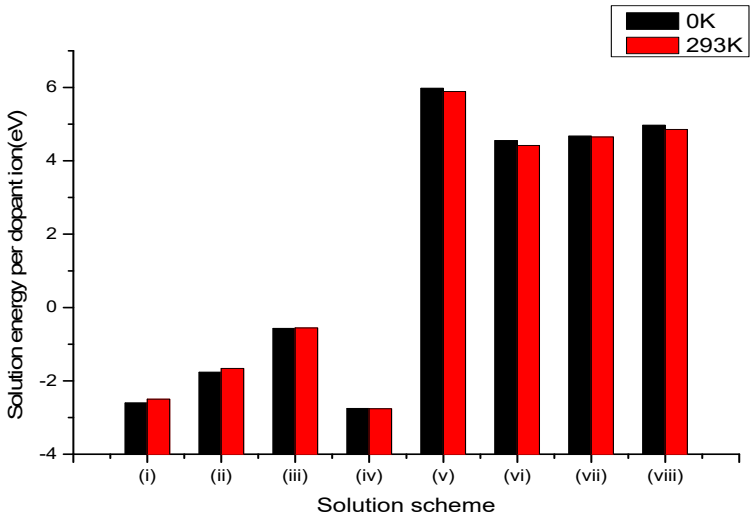

Figure 1. Bar chart of solution energies vs. solution schemes for divalent dopant (V^{2+}) at the Li and Nb sites, considering the first neighbours in relation to the c axis.

3.2.2. Trivalent Dopants

As with the divalent ion V^{2+}, the trivalent V^{3+} and Mo^{3+} dopants can be incorporated at the lithium and niobium sites in the $LiNbO_3$ matrix through various schemes as shown in Tables 4 and 5. When these ions are substituted at Li and Nb sites, the extra positive charge can, as noted earlier, be compensated by the creation of vacancies, interstitials, anti-site defects or self-compensation.

Table 4. Types of defects considered due to V^{3+} incorporation in $LiNbO_3$.

Site	Charge Compensation	Reaction
Li^+	Lithium Vacancies	(i) $0.5M_2O_3+3Li_{Li} \rightarrow M_{Li}+2V'_{Li}+1.5Li_2O$
	Niobium Vacancies	(ii) $2.5M_2O_3+5Li_{Li}+2Nb_{Nb} \rightarrow 5M_{Li}+2V''''_{Nb}+2.5Li_2O+Nb_2O_5$
	Oxygen Interstitial	(iii) $0.5M_2O_3+Li_{Li} \rightarrow M_{Li}+O''_i+0.5Li_2O$
Li^+ and Nb^{5+}	Self-Compensation	(iv) $M_2O_3+Li_{Li}+Nb_{Nb} \rightarrow M_{Li}+M''_{Nb}+0.5Li_2O+0.5\,Nb_2O_5$
Nb^{5+}	Oxygen Vacancies	(v) $0.5M_2O_3+Nb_{Nb}+O_O \rightarrow M''_{Nb}+V_O+0.5Nb_2O_5$
	Anti-site (Nb_{Li})	(vi) $M_2O_3+Li_{Li}+2Nb_{Nb} \rightarrow 2M''_{Nb}+Nb_{Li}+LiNbO_3$
	Lithium Vacancies and Anti-site (Nb_{Li})	(vii) $0.5M_2O_3+3Li_{Li}+Nb_{Nb} \rightarrow M''_{Nb}+2V'_{Li}+Nb_{Li}+1.5Li_2O$

Table 5. Types of defects considered due to Mo^{3+} incorporation in $LiNbO_3$.

Site	Charge Compensation	Reaction
Li^+	Lithium Vacancies	(i) $LiMoO_2+3Li_{Li} \rightarrow Mo_{Li}+2V'_{Li}+2Li_2O$
	Niobium Vacancies	(ii) $5LiMoO_2+5Li_{Li}+2Nb_{Nb} \rightarrow 5Mo_{Li}+2V''''_{Nb}+5Li_2O+Nb_2O_5$
	Oxygen Interstitial	(iii) $LiMoO_2+Li_{Li} \rightarrow Mo_{Li}+O''_i+Li_2O$
Li^+ and Nb^{5+}	Self-Compensation	(iv) $2LiMoO_2+2Li_{Li}+Nb_{Nb} \rightarrow Mo_{Li}+Mo''_{Nb}+1.5Li_2O+0.5Nb_2O_5$
Nb^{5+}	Oxygen Vacancies	(v) $LiMoO_2+Nb_{Nb}+O_O \rightarrow Mo''_{Nb}+V_O+0.5Li_2O+0.5Nb_2O_5$
Nb^{5+}	Anti-site (Nb_{Li})	(vi) $2LiMoO_2+Li_{Li}+2Nb_{Nb} \rightarrow 2Mo''_{Nb}+Nb_{Li}+1.5Li_2O+0.5Nb_2O_5$
Nb^{5+}	Lithium Vacancies and Anti-site (Nb_{Li})	(vii) $LiMoO_2+3Li_{Li}+Nb_{Nb} \rightarrow Mo''_{Nb}+2V'_{Li}+Nb_{Li}+2Li_2O$

According to Figures 2 and 3 for the first and second neighbours with respect to the c axis, the trivalent V^{3+} and Mo^{3+} ions prefer to occupy both the Li and Nb sites according to scheme (iv) which is also observed in other trivalent ions [23–25]. This can be attributed to the similarity between the ionic radius of V^{3+} which is 0.64 Å and Mo^{3+} which is 0.67 Å [40] and that of Li^+ and Nb^{5+}. The ionic radius of Li^+ varies between 0.59 Å and 0.74 Å and Nb^{5+} varies from 0.32 Å to 0. 66 Å [40]. All these ionic radii are in relation to the coordination sphere with oxygen atoms.

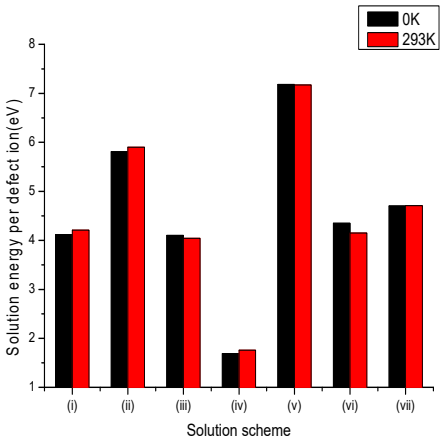

Figure 2. Bar chart of solution energies vs. solution schemes for trivalent dopant (V^{3+}) at the Li and Nb sites, considering the first neighbours in relation to the c axis.

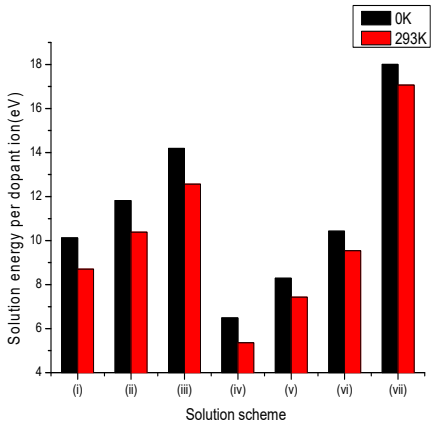

Figure 3. Bar chart of solution energies vs. solution schemes for trivalent dopant (Mo^{3+}) at the Li and Nb sites, considering the first neighbours in relation to the c axis.

3.2.3. Tetravalent Dopants

Like other divalent and trivalent cations, tetravalent V^{4+} and M^{4+} dopant ions can also substitute at either the Li^+ or Nb^{5+} sites. When these ions substitute at the Li^+ and Nb^{5+} site charge compensation is required, and various schemes involving vacancies, interstitials, anti-sites and self-compensation are adopted, as shown in Tables 6 and 7.

Table 6. Types of defects considered due to M = V^{4+} incorporation in $LiNbO_3$.

Site	Charge Compensation	Reaction
Li^+	Lithium Vacancies	(i) $MO_2+4Li_{Li} \rightarrow M_{Li}+3V'_{Li} + 2Li_2O$
	Niobium Vacancies	(ii) $5MO_2+5Li_{Li}+3Nb_{Nb} \rightarrow 5M_{Li}+3V''''''_{Nb} + 2.5Li_2O+1.5Nb_2O_5$
	Oxygen Interstitial	(iii) $2MO_2+2Li_{Li} \rightarrow 2M_{Li}+3O''_i+Li_2O$
Li^+ and Nb^{5+}	Self-Compensation	(iv) $4MO_2+Li_{Li}+3Nb_{Nb} \rightarrow M_{Li}+3M'_{Nb} + 0.5Li_2O+1.5\ Nb_2O_5$
Nb^{5+}	Anti-site (Nb_{Li})	(v) $4MO_2+Li_{Li}+4Nb_{Nb} \rightarrow 4M'_{Nb}+Nb_{Li}+0.5Li_2O+1.5Nb_2O_5$
	Lithium Vacancies and Anti-site (Nb_{Li})	(vi) $MO_2+4Li_{Li}+Nb_{Nb} \rightarrow M'_{Nb}+3V'_{Li}+Nb_{Li}+2Li_2O$
		(vii) $2MO_2+3Li_{Li}+2Nb_{Nb} \rightarrow 2M'_{Nb}+2V'_{Li}+Nb_{Li}+Li_2O+LiNbO_3$
		(viii) $3MO_2+2Li_{Li}+3Nb_{Nb} \rightarrow 3M'_{Nb}+V'_{Li}+Nb_{Li}+LiNbO_3$
	Oxygen Vacancies	(ix) $2MO_2+2Nb_{Nb}+O_O \rightarrow 2M'_{Nb}+V_O+Nb_2O_5$

Table 7. Types of defects considered due to M=Mo^{4+} incorporation in $LiNbO_3$.

Site	Charge Compensation	Reaction
Li^+	Lithium Vacancies	(i) $Li_2MoO_3+4Li_{Li} \rightarrow Mo_{Li}+3V'_{Li} + 3Li_2O$
	Niobium Vacancies	(ii) $5Li_2MoO_3+5Li_{Li}+3Nb_{Nb} \rightarrow 5Mo_{Li}+3V''''''_{Nb} + 7.5Li_2O+1.5Nb_2O_5$
	Oxygen Interstitial	(iii) $2Li_2MoO_3+2Li_{Li} \rightarrow 2Mo_{Li}+3O''_i+3Li_2O$
Li^+ and Nb^{5+}	Self-Compensation	(iv) $4Li_2MoO_3+Li_{Li}+3Nb_{Nb} \rightarrow Mo_{Li}+3Mo'_{Nb} + 4.5Li_2O+1.5\ Nb_2O_5$
Nb^{5+}	Anti-site (Nb_{Li})	(v) $4Li_2MoO_3+Li_{Li}+4Nb_{Nb} \rightarrow 4Mo'_{Nb}+Nb_{Li}+4.5Li_2O+1.5Nb_2O_5$
	Lithium Vacancies and Anti-site (Nb_{Li})	(vi) $Li_2MoO_3+4Li_{Li}+Nb_{Nb} \rightarrow Mo'_{Nb}+3V'_{Li}+Nb_{Li}+3Li_2O$
		(vii) $2Li_2MoO_3+3Li_{Li}+2Nb_{Nb} \rightarrow 2Mo'_{Nb}+Nb_{Li}+2V'_{Li}+3Li_2O+LiNbO_3$
		(viii) $3Li_2MoO_3+2Li_{Li}+3Nb_{Nb} \rightarrow 3Mo'_{Nb}+Nb_{Li}+V'_{Li}+3Li_2O+2LiNbO_3$
	Oxygen Vacancies	(ix) $2Li_2MoO_3+2Nb_{Nb}+O_O \rightarrow 2Mo'_{Nb}+V_O+2Li_2o+Nb_2O_5$

The results obtained from these calculations are given in Figures 4 and 5. By inspecting these figures, it can be seen that the tetravalent cation V^{4+} prefers to be incorporated at the Li^+ and Nb^{5+} sites through scheme (iv), while the Mo^{4+} ion prefers to be incorporated at the niobium site compensated by an oxygen vacancy according to scheme (ix). Similar to the divalent and trivalent dopants, this preference is related to the proximity with the ionic radii of Li^+ and Nb^{5+}.

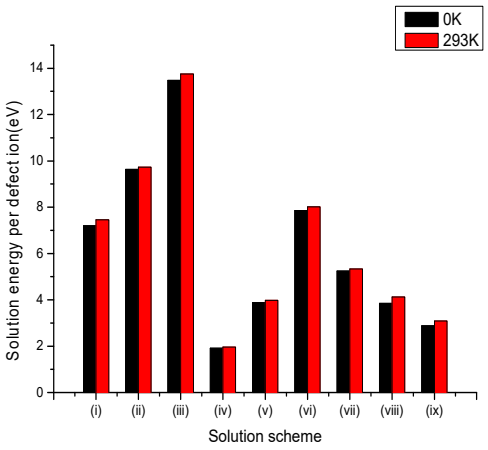

Figure 4. Bar chart of solution energies vs. solution schemes for tetravalent dopant (V^{4+}) at the Li and Nb sites, considering the first neighbours in relation to the c axis.

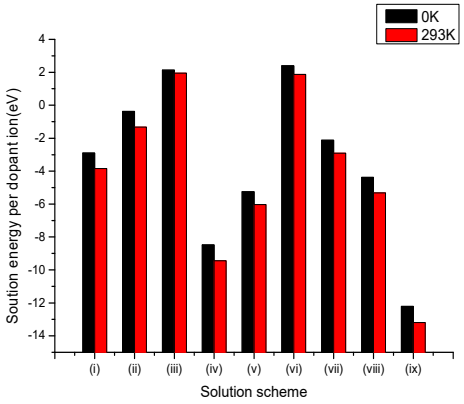

Figure 5. Bar chart of solution energies vs. solution schemes for tetravalent dopant (Mo^{4+}) at the Li and Nb sites, considering the first neighbours in relation to the c axis.

3.2.4. Pentavalent Dopants

For the pentavalent dopants V^{5+} and Mo^{5+}, no charge compensation is required for the substitution at the Nb^{5+} host site, but it is required when the substitution is at the Li^{+} host site, as shown in Tables 8 and 9.

Table 8. Types of defects considered due to M = V^{5+} incorporation in $LiNbO_3$.

Site	Charge Compensation	Reaction
Li^{+}	Lithium Vacancies	**(i)** $0.5M_2O_5+5Li_{Li} \rightarrow M_{Li}+4V'_{Li}+2.5Li_2O$
	Niobium Vacancies	**(ii)** $2.5M_2O_5+5Li_{Li}+5Nb_{Nb} \rightarrow 5M_{Li}+4V''''_{Nb}+2.5Li_2O+2Nb_2O_5$
	Oxygen Interstitial	**(iii)** $0.5M_2O_5+Li_{Li} \rightarrow M_{Li}+2O''_i+0.5Li_2O$
Nb^{5+}	No Charge Compensation	**(iv)** $0.5M_2O_5+Nb_{Nb} \rightarrow M_{Nb}+0.5Nb_2O_5$

Table 9. Types of defects considered due to Mo^{5+} incorporation in $LiNbO_3$.

Site	Charge Compensation	Reaction
Li^{+}	Lithium Vacancies	**(i)** $Li_3MoO_4+5Li_{Li} \rightarrow Mo_{Li}+4V'_{Li}+4Li_2O$
	Niobium Vacancies	**(ii)** $5Li_3MoO_4+5Li_{Li}+4Nb_{Nb} \rightarrow 5Mo_{Li}+4V''''_{Nb}+10Li_2O+2Nb_2O_5$
	Oxygen Interstitial	**(iii)** $Li_3MoO_4+Li_{Li} \rightarrow Mo_{Li}+2O''_i+2Li_2O$
Nb^{5+}	No Charge Compensation	**(iv)** $Li_3MoO_4+Nb_{Nb} \rightarrow Mo_{Nb}+1.5Li_2O+0.5Nb_2O_5$

The solution energies for the pentavalent (V^{5+}) and (Mo^{5+}) dopants with different charge compensation mechanisms were evaluated and plotted as a function of the reaction scheme. Based on

the lowest energy value, it seems that the incorporation of pentavalent (V^{5+}) and (Mo^{5+}) ions at an Nb site is energetically more favourable than at an Li site, according to scheme (iv) as shown in Figures 6 and 7 at temperatures 0 K and 293 K. This can be attributed to the similarity between the charge of the V^{5+} and Mo^{5+} ions and the Nb^{5+} host, which can contribute to a small deformation in the lattice and consequently a lower solution energy. Experimental results by Kong et al. [17] and Tian et al. [16] show that substitution occurs at the Nb^{5+} site.

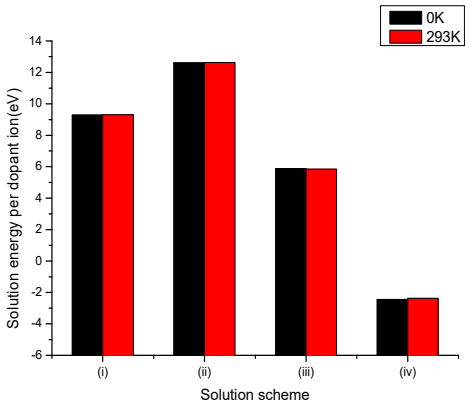

Figure 6. Bar chart of solution energies vs. solution schemes for pentavalent dopant (V^{5+}) at the Li and Nb sites, considering the first neighbours in relation to the c axis.

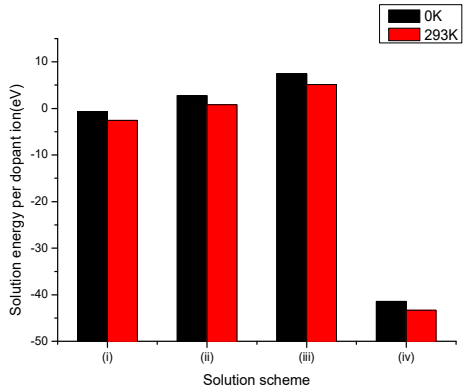

Figure 7. Bar chart of solution energies vs. solution schemes for pentavalent dopant (Mo^{5+}) at the Li and Nb sites, considering the first neighbours in relation to the c axis.

3.2.5. Hexavalent Dopants

For the hexavalent dopant Mo^{6+}, as with the pentavalent ions, there is no self-compensation mechanism and charge compensation schemes are possible when replacing Li and Nb in the $LiNbO_3$ matrix as shown in Table 10.

Table 10. Types of defects considered due to Mo^{6+} incorporation in $LiNbO_3$.

Site	Charge Compensation	Reaction
Li^+	**Lithium Vacancies**	**(i)** $Li_2MoO_4 + 6Li_{Li} \rightarrow Mo_{Li} + 5V'_{Li} + 4Li_2O$
	Niobium Vacancies	**(ii)** $Li_2MoO_4 + Li_{Li} + Nb_{Nb} \rightarrow Mo_{Li} + V''''_{Nb} + 1.5Li_2O + 0.5Nb_2O_5$
	Oxygen Interstitial	**(iii)** $2Li_2MoO_4 + 2Li_{Li} \rightarrow 2Mo_{Li} + 5O''_i + 3Li_2O$
Nb^{5+}	**Lithium Vacancies**	**(iv)** $Li_2MoO_4 + Li_{Li} + Nb_{Nb} \rightarrow Mo_{Nb} + V'_{Li} + 1.5Li_2O + 0.5Nb_2O_5$
	Niobium Vacancies	**(v)** $5Li_2MoO_4 + 6Nb_{Nb} \rightarrow 5Mo_{Nb} + V''''_{Nb} + 5Li_2O + 3Nb_2O_5$
	Oxygen Interstitial	**(vi)** $2Li_2MoO_4 + 2Nb_{Nb} \rightarrow 2Mo_{Nb} + O''_i + 2Li_2O + Nb_2O_5$

The solution energies for the hexavalent (Mo^{6+}) dopants with different charge-compensation mechanisms were evaluated and plotted as a function of the reaction scheme. Based on the lowest

energy value, it seems that the incorporation of hexavalent (Mo^{6+}) ions at an Nb site is energetically more favourable than at an Li site, according to scheme (iv) as shown in Figure 8 at temperatures 0 K and 293 K. This can be attributed to the similarity between the ionic radii of Mo^{6+} ions and the Nb^{5+} host site (0.32–0.71 Å) [40]. The ionic radii of Mo^{6+}, taking into account the coordination number, vary between 0.42 and 0.67 Å [40], and the small difference between the Mo^{6+} dopant ions and Nb^{5+} ions can contribute to a small deformation in the lattice and consequently a lower solution energy. This result reveals that global trends of dopant solution energies are controlled by the combination of dopant ion size [40] and its electrostatic interactions, demonstrating that there is a relation between the energetically preferred site and the types of defect mechanisms involved in the doping process. Experimental results from Kong et al. [17] and Zhu et al. [41] show that substitution occurs at the Nb^{5+} site.

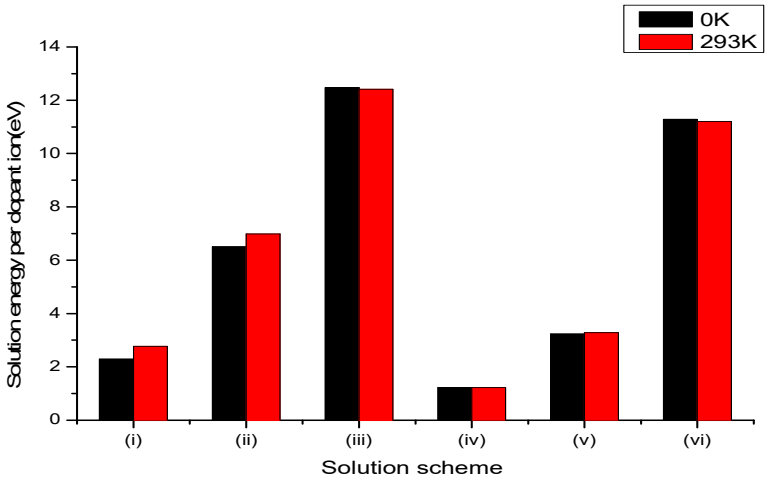

Figure 8. Bar chart of solution energies vs. solution schemes for hexavalent dopant (Mo^{6+}) at the Li and Nb sites, considering the first neighbours in relation to the c axis.

In all cases, the energy involved in doping was obtained by calculating the solution energy, which includes all terms of the thermodynamic cycle involved in the solution process. For example, the solution energy, E_{sol}, corresponding to the incorporation of V^{2+} at the Li^{+} site (second equation in Table 3) is given by:

$$E_{Sol} = E_{Def}(5M_{Li} + V''''''_{Nb}) + 2.5E_{Latt}(Li_2O) + 0.5E_{Latt}(Nb_2O_5) - 5E_{Latt}(MO) \quad (2)$$

where the E_{latt} and E_{Def} terms are lattice energies and defect energy.

All energies were normalised by the number of dopants, i.e., the solution energy is divided by the number of dopants involved. For example, for scheme (ii) of Table 3, the energy must be divided by five, since five lithium sites are occupied. This is done because the number of dopants varies for each mechanism. Lattice energies, E_{latt}, required to calculate the solution energies are given in Table 11.

Table 11. Lattice energies used in the solution energy calculations (eV).

Compound	Lattice Energy	Lattice Energy
	0 K	**293 K**
$LiNbO_3$	−174.45	−174.66
Li_2O	−33.16	−32.92
Nb_2O_5	−314.37	−313.39
VO	−22.06	−22.07
V_2O_3	−124.37	−124.39
VO_2	−111.54	−111.57
V_2O_5	−315.65	−274.18
$LiMoO_2$	−98.07	−97.09
Li_2MoO_3	−150.38	−149.10
Li_3MoO_4	−181.28	−178.88
Li_2MoO_4	−234.06	−234.12

3.2.6. Summary of Results for Vanadium and Molybdenum Dopants in $LiNbO_3$

In this sub-section, the results presented in the last five subsections are summarised.

Divalent dopants: the calculations predict that, for V^{2+}, self-compensation (simultaneous doping at lithium and niobium sites) and doping at the lithium site with lithium vacancy compensation are most likely. It is noted that V^{2+}_{Li} defects have been observed experimentally [18].

Trivalent dopants: both V^{3+} and Mo^{3+} ions are predicted to self-compensate. Experimental data from [18] support V^{3+} doping at the lithium site, as with V^{2+}.

Tetravalent dopants: here, different behaviour is predicted for vanadium and molybdenum. V^{4+} is predicted to self-compensate, while Mo^{4+} is predicted to occupy a niobium site with oxygen vacancy charge compensation. Again, [18] suggests that V^{4+} can dope at a lithium site.

Pentavalent dopants: both V^{5+} and Mo^{5+} are predicted to dope at the niobium site (no charge compensation is needed), agreeing with experimental results [16,17].

Hexavalent dopants: Mo^{6+} is predicted to dope at the niobium site, with charge compensation by lithium vacancy formation. The occupation of the niobium site is supported by experimental data [16,17,19].

4. Conclusions

This paper has presented a computational study of VO, V_2O_3, VO_2 and V_2O_5 as well as $LiMoO_2$, Li_2MoO_3, Li_3MoO_4 and Li_2MoO_4 structures doped into $LiNbO_3$. New interatomic potential parameters for VO, V_2O_3, VO_2 and V_2O_5 as well as $LiMoO_2$, Li_2MoO_3, Li_3MoO_4 and Li_2MoO_4 have been developed. It was found that divalent (V^{2+}), trivalent (V^{3+}, Mo^{3+}) and tetravalent (V^{4+}) ions are more favourably incorporated at the Li and Nb sites through the self-compensation mechanism. The tetravalent (Mo^{4+}) ion is more favourably incorporated at the niobium site, compensated by an oxygen vacancy. The pentavalent ions (V^{5+}, Mo^{5+}) and hexavalent (Mo^{6+}) ion are more favourably incorporated at the Nb site, and the lowest energy schemes involve, respectively, no charge compensation, and for the Mo^{6+} ion, charge compensation with lithium vacancy. This is shown to be consistent with some experimental data, although future calculations involving finite V^{5+} and Mo^{6+} concentrations will be carried out to investigate this further.

Finally, to summarise, in this paper we have looked in detail at vanadium and molybdenum dopants in various charge states in $LiNbO_3$, and through the use of solution energies, identified the energetically favoured sites and charge compensation mechanisms, while comparing the results with available experimental and theoretical work in this field.

Author Contributions: Conceptualisation, R.M.A.; Data curation, R.M.A. and E.F.d.S.M.; Formal analysis, R.A.J.; Supervision, M.E.G.V. and R.A.J.; Validation, M.E.G.V. and R.A.J.; Writing—original draft, R.M.A.; Writing—review & editing, M.E.G.V. and R.A.J. All authors have read and agreed to the published version of the manuscript.

Funding: This research received no external funding.

Acknowledgments: The authors would like to thank the peer reviewers, whose detailed comments have undoubtedly led to major improvements to this paper.

Conflicts of Interest: The authors declare no conflict of interest.

References

1. Mandula, G.; Rupp, R.A.; Balaskó, M.; Kovács, L. Decay of photorefractive gratings in $LiNbO_3$:Fe by neutron irradiation. *Appl. Phys. Lett.* **2005**, *86*, 141107. [CrossRef]
2. Ionita, I.; Jaque, F. Photoconductivity and electron mobility in $LiNbO_3$ co-doped with Cr^{3+} and MgO. *Opt. Mater.* **1998**, *10*, 171–173. [CrossRef]
3. Kaczmarec, S.M.; Bodziony, T. Low symmetry centers in $LiNbO_3$ with Yb and Er. *J. Non-Cryst. Solids* **2008**, *354*, 4202–4210. [CrossRef]
4. Kokanyan, E.P.; Razzari, L.; Cristiani, I.; Degiorgio, V.; Gruber, J.B. Reduced photorefraction in hafnium-doped single-domain and periodically poled lithium niobate crystals. *Appl. Phys. Lett.* **2004**, *84*, 1880. [CrossRef]
5. Corradi, G.; Meyer, M.; Kovács, L.; Polgár, K. Gap levels of Ti^{3+} on Nb or Li sites in $LiNbO_3$:(Mg):Ti crystals and their effect on charge transfer processes. *Appl. Phys. B* **2004**, *78*, 607–614. [CrossRef]
6. Cantelar, E.; Quintanilla, M.; Pernas, P.L.; Torchia, G.A.; Lifante, G.; Cussó, F. Polarized emission and absorption cross-section calculation in $LiNbO_3$:Tm^{3+}. *J. Lumin.* **2008**, *128*, 988–991. [CrossRef]
7. Shura, J.W.; Shina, T.I.; Leea, S.M.; Baekb, S.W.; Yoon, D.H. Photoluminescence properties of Nd: $LiNbO_3$ co-doped with ZnO fiber single crystals grown by micro-pulling-down method. *Mater. Sci. Eng. B* **2003**, *105*, 16–19. [CrossRef]
8. Li, S.; Liu, S.; Kong, Y.; Deng, D.; Gao, G.; Li, Y.; Gao, H.; Zhang, L.; Hang, Z.; Chen, S.; et al. The optical damage resistance and absorption spectra of $LiNbO_3$:Hf crystals. *J. Phys. Condens. Matter* **2006**, *18*, 3527–3534. [CrossRef]
9. Hesselink, L.; Orlov, S.S.; Liu, A.; Akella, A.; Lande, D.; Neurgaonkar, R.R. Photorefractive materials for nonvolatile volume holographic data storage. *Science* **1998**, *282*, 1089–1094. [CrossRef]
10. Camarillo, E.; Murrieta, H.; Hernandez, J.M.; Zoilo, R.; Flores, M.C.; Han, T.P.J.; Jaque, F. Optical properties of $LiNbO_3$:Cr crystals co-doped with germanium oxide. *J. Lumin.* **2008**, *128*, 747–750. [CrossRef]
11. Luo, S.; Meng, Q.; Wang, J.; Sun, X. Effect of In^{3+} concentration on the photorefraction and scattering properties in In: Fe:Cu:$LiNbO_3$ crystals at 532 nm wavelength. *Opt. Commun.* **2016**, *358*, 198–201. [CrossRef]
12. Nie, Y.; Wang, R.; Wang, B. Growth and holographic storage properties of In:Ce:Cu:$LiNbO_3$ crystal. *Mater. Chem. Phys.* **2007**, *102*, 281–283. [CrossRef]
13. Zhen, X.H.; Li, H.T.; Sun, Z.J.; Ye, S.J.; Zhao, L.C.; Xu, Y.H. Holographic properties of double-doped Zn:Fe:$LiNbO_3$ crystals. *Mater. Lett.* **2004**, *58*, 1000–1002. [CrossRef]
14. Wei, Z.; Naidong, Z.; Qingquan, L. Growth and Holographic Storage Properties of Sc, Fe Co-Doped Lithium Niobate Crystals. *J. Rare Earth* **2007**, *25*, 775–778. [CrossRef]
15. Xu, C.; Leng, X.; Xu, L.; Wen, A.; Xu, Y. Enhanced nonvolatile holographic properties in Zn, Ru and Fe co-doped $LiNbO_3$ crystals. *Opt. Commun.* **2012**, *285*, 3868–3871. [CrossRef]
16. Tian, T.; Kong, Y.; Liu, S.; Li, W.; Wu, L.; Chen, S.; Xu, J. The photorefraction of molybdenum-doped lithium niobate crystals. *Opt. Lett.* **2012**, *37*, 2679–2681. [CrossRef]
17. Kong, Y.; Liu, S.; Xu, J. Recent Advances in the Photorefraction of Doped Lithium Niobate Crystals. *Materials* **2012**, *5*, 1954–1971. [CrossRef]
18. Saeed, S.; Zheng, D.; Liu, H.; Xue, L.; Wang, W.; Zhu, L.; Hu, M.; Liu, S.; Chen, S.; Zhang, L.; et al. Rapid response of photorefraction in vanadium and magnesium co-doped lithium niobate. *J. Phys. D Appl. Phys.* **2019**, *52*, 405303. [CrossRef]
19. Xue, L.; Liu, H.; Zheng, D.; Saeed, S.; Wang, X.; Tian, T.; Zhu, L.; Kong, Y.; Liu, S.; Chen, S.; et al. The Photorefractive Response of Zn and Mo Codoped $LiNbO_3$ in the Visible Region. *Crystals* **2019**, *9*, 228. [CrossRef]

20. Fan, Y.; Li, L.; Li, Y.; Sun, X.; Zhao, X. Hybrid density functional theory study of vanadium doping in stoichiometric and congruent $LiNbO_3$. *Phys. Rev. B* **2019**, *99*, 035147. [CrossRef]
21. Wang, W.; Liu, H.; Zheng, D.; Kong, Y.; Zhang, L.; Xu, J. Interaction between Mo and intrinsic or extrinsic defects of Mo doped $LiNbO_3$ from first-principles calculations. *J. Phys. Condens. Matter* **2020**, *32*, 255701. [CrossRef] [PubMed]
22. Jackson, R.A.; Valerio, M.E.G. A new interatomic potential for the ferroelectric and paraelectric phases of $LiNbO_3$. *J. Phys. Condens. Matter* **2005**, *17*, 837. [CrossRef]
23. Araujo, R.M.; Lengyel, K.; Jackson, R.A.; Valerio, M.E.G.; Kovacs, L. Computer modelling of intrinsic and substitutional defects in $LiNbO_3$. *Phys. Status Solidi* **2007**, *4*, 1201–1204.22. [CrossRef]
24. Araujo, R.M.; Lengyel, K.; Jackson, R.A.; Kovacs, L.; Valerio, M.E.G. A computational study of intrinsic and extrinsic defects in $LiNbO_3$. *J. Phys. Condens. Matter* **2007**, *19*, 046211. [CrossRef]
25. Araujo, R.M.; Valerio, M.E.G.; Jackson, R.A. Computer modelling of trivalent metal dopants in lithium niobite. *J. Phys. Condens. Matter* **2008**, *20*, 035201. [CrossRef]
26. Araujo, R.M.; Valerio, M.E.G.; Jackson, R.A. Computer simulation of metal co-doping in lithium niobate. *Proc. R. Soc. A* **2014**, *470*, 0406. [CrossRef]
27. Araujo, R.M.; Valerio, M.E.G.; Jackson, R.A. Computer Modelling of Hafnium Doping in Lithium Niobate. *Crystals* **2018**, *8*, 123. [CrossRef]
28. Mott, N.F.; Littleton, M.J. Conduction in polar crystals. Electrolytic conduction in solid salts. *Trans. Faraday Soc.* **1938**, *34*, 485–499. [CrossRef]
29. Sanders, M.J.; Leslie, M.; Catlow, C.R.A. Interatomic potentials for SiO_2. *J. Chem. Soc. Chem. Commun.* **1984**, 1271–1273. [CrossRef]
30. Dick, B.J.; Overhauser, A.W. Theory of the dielectric constants of alkali halide crystals. *Phys. Rev.* **1958**, *112*, 90. [CrossRef]
31. Taylor, D. Thermal expansion data. I: Binary oxides with the sodium chloride and wurtzite structures, MO. *Trans. J. Br. Ceram. Soc.* **1984**, *83*, 5–9.
32. Luedtke, T.; Weber, D.; Schmidt, A.; Mueller, A.; Reimann, C.; Becker, N.; Bredow, T.; Dronskowski, R.; Ressler, T.; Lerch, M. Synthesis and characterization of metastable transition metal oxides and oxide nitrides. *Z. Fuer Krist. Cryst. Mater.* **2017**, *232*, 3–14. [CrossRef]
33. McWhan, D.B.; Marezio, M.; Remeika, J.P.; Dernier, P.D. X-ray diffraction study of metallic VO_2. *Phys. Rev. B Solid State* **1974**, *10*, 490–495. [CrossRef]
34. Balog, P.; Orosel, D.; Cancarevic, Z.; Schoen, C.; Jansen, M. V_2O_5 phase diagram revisited at high pressures and high temperatures. *J. Alloy. Compd.* **2007**, *429*, 87–98. [CrossRef]
35. Aleandri, L.E.; McCarley, R.E. Hexagonal lithium molybdate, $LiMoO_2$: A close-packed layered structure with infinite molybdenum-molybdenum-bonded sheets. *Inorg. Chem.* **1988**, *27*, 1041–1044. [CrossRef]
36. Hibble, S.J.; Fawcett, I.D.; Hannon, A.C. Structure of Two Disordered Molybdates, $Li_2Mo^{IV}O_3$ and $Li_4Mo_3{}^{IV}O_8$, from Total Neutron Scattering. *Acta Crystallogr. Sect. B Struct. Sci.* **1997**, *53*, 604–612. [CrossRef]
37. Mikhailova, D.; Voss, A.; Oswald, S.; Tsirlin, A.A.; Schmidt, M.; Senyshyn, A.; Eckert, J.; Ehrenberg, H. Lithium Insertion into Li_2MoO_4: Reversible Formation of $(Li_3Mo)O_4$ with a Disordered Rock-Salt Structure. *Chem. Mater.* **2015**, *27*, 4485–4492. [CrossRef]
38. Kolitsch, U. The crystal structures of phenacite-type $Li_2(MoO_4)$, and scheelite-type $LiY(MoO_4)_2$ and $LiNd(MoO_4)_2$. *Z. Fuer Krist.* **2001**, *216*, 449–454. [CrossRef]
39. Kröger, F.A.; Vink, H.J. The origin of the fluorescence in self-activated ZnS, CdS, and ZnO. *J. Chem. Phys.* **1954**, *22*, 250. [CrossRef]
40. Shannon, R.D.; Prewitt, C.T. Revised values of effective ionic radii. *Acta Crystallogr. Sect. B Struct. Crystallogr. Cryst. Chem.* **1969**, *26*, 1046–1048. [CrossRef]
41. Zhu, L.; Zheng, D.; Saeed, S.; Wang, S.; Liu, H.; Kong, Y.; Liu, S.; Chen, S.; Zhang, L.; Xu, J. Photorefractive Properties of Molybdenum and Hafnium Co-Doped $LiNbO_3$. *Crystals* **2018**, *8*, 322. [CrossRef]